Wideband Synthetic Aperture Test Bed for Intelligent Reflecting Surfaces

Peter Vouras, Mohamed Kashef (Hany), Sudantha Perera, Carnot Nogueira, Richard Candell, Kate A. Remley

***Abstract*—This paper describes a spherical beamforming implementation for wideband synthetic aperture channel sounders that can be used to predict the scattering performance of an Intelligent Reflection Surface (IRS). An IRS creates controlled propagation conditions in wireless channels that can amplify the signal power available at a receiver or can enhance communications security by reducing the signal leaking to an eavesdropper. Most IRS performance evaluations described in the technical literature to date rely on simulation and modeling approaches. These techniques necessarily produce idealized results that neglect the impact of real-world multipath. However, by incorporating wireless channel measurements taken by a synthetic aperture into a spherical beamforming framework, the detrimental effects of environmental multipath on the signal reflected from an IRS can be realistically accounted for.**

I. Introduction

A key enabling technology for sixth-generation (6G) wireless communication networks is the use of Intelligent Reflecting Surfaces (IRSs) that can passively reflect transmitted signals to focus energy towards the receiver. Phase shifted and attenuated signals reflected from the IRS combine coherently in space with the direct signal to create increased signal power at the receiver's location. To successfully control passive signal reflections in a wireless channel, many complicated environmental variables must be manipulated. First, the ambient propagation channel must be accurately estimated and an appropriate phase shift must be computed and applied to the signal reflected from each individual element of an IRS. To compute the correct phase shifts, the angles of arrival at the IRS for specular multipath sources and the line-of-sight (LOS) transmitted signal must be determined.

Synthetic aperture channel sounders provide excellent angle resolution and multipath estimation performance to help determine the optimal configuration for an IRS but they typically rely on conventional wideband beamforming. Wideband beamforming eliminates beam squint by implementing a true time delay behind each spatial sample of a synthetic aperture. Wideband beamforming however will not yield the most accurate estimates for multipath angles of arrival unless it accounts for the spherical curvature of the wavefronts propagating across the aperture observation plane. This paper describes a beamforming implementation that accounts for the spherical wavefront of propagating waves and yields more accurate power delay profiles (PDPs) and delay slices that characterize the channel impulse response. As a result of the increased beamforming accuracy, all the energy reflected from an IRS and arriving at the receiver can be better predicted.

P. V. is with the United States Department of Defense, Washington, DC, 20375 USA, e-mail: synthetic_aperture_twg@ieee.org.

M. K. and R. C. are with the National Institute of Standards and Technology (NIST), Gaithersburg, MD, 20899 USA e-mail: mohamed.kashef, richard.candell@nist.gov.

S. P., C. N., and K. A. R. are with the National Institute of Standards and Technology (NIST), Boulder, CO, 80303 USA e-mail: sudantha.perera, carnot.nogueira, kate.remley@nist.gov.

II. Intelligent Reflecting Surfaces

In general, an IRS is a planar surface with a large number of passive reflecting elements embedded in it. Each element is able to impart an independent phase or attenuation to the incident signal before it is reflected. By adjusting the phase shifts of the IRS elements, reflected signals can be constructively superimposed with those from the line-of-sight path to enhance signal power at the receiver. Alternatively, the IRS can also be configured to reflect a signal that destructively cancels unwanted interference at the receiver or any signal leakage available to eavesdroppers. The ability to dynamically reconfigure wireless channels using an IRS offers a quantum leap in wireless link reliability, especially for industrial environments where many highly-reflective objects, such as metal robots, may be in motion.

An IRS possesses several practical manufacturing advantages. Foremost, the individual reflecting elements are passive printed dipoles and can reflect impinging signals without requiring any active transmit channels. Thus, they are orders of magnitude cheaper than active phased arrays or active reflecting surfaces. Furthermore, an IRS is generally lightweight and can be easily mounted on walls or other surfaces. Thus, IRSs can be mass produced and massively deployed in wireless networks. The degrees of freedom (amplitude and phase) available for optimization at each IRS element and the large size of the surface create a complex computational problem when designing the IRS reflection characteristics as well as for predicting the final signal at the intended receiver [1]–[10].

When a plane wave is incident on a large, homogeneous, flat surface, energy will reflect in another direction as determined by Snell's law. Parallel incident rays will remain parallel after reflection. In contrast, an IRS of the same physical dimensions can be configured to synthesize the shape of a different object (e.g., a parabolic reflector), thereby controlling the directivity of the reflected waveform. Similar to the operation of an IRS, Fig. 1 illustrates the phase measured at the discrete spatial locations of a planar synthetic aperture. The phase shown at each spatial sample is identical to the received signal phase seen by each element of an IRS.

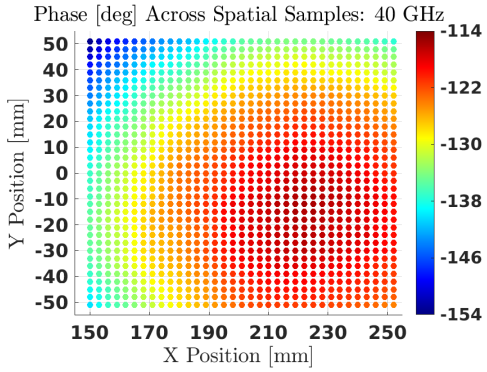

Fig. 1: Measured phase across synthetic aperture

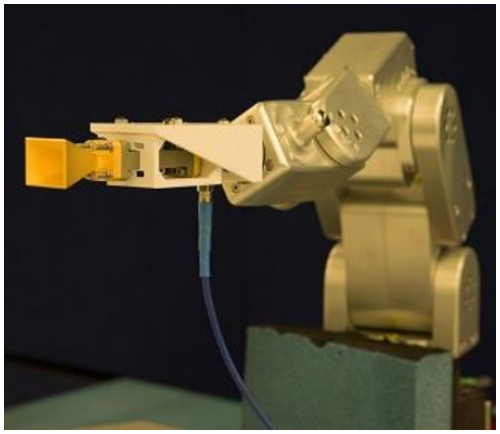

Fig. 2: Synthetic aperture channel sounder created by mounting antenna on robot

Channel modeling for IRSs is nascent and evolving with very limited empirical results to date. In a multipath scattering environment, different portions of the IRS will observe various linear combinations of the impinging waves, leading to fading variations. The wavelength limits the variability so even in rich scattering environments there will be correlation between the channel coefficients observed at IRS elements spaced a few wavelengths apart. This fading property will affect IRS operation in multiple ways. First, it enables an IRS to reflect multiple signals to different locations simultaneously, thereby creating communication links to multiple users. Second, fading across the aperture also affects how the IRS will interact with interfering signals.

III. Synthetic Aperture Channel Sounders

The simplest channel sounding systems rely on directional antennas placed in a bistatic geometry to transmit and receive a probe signal that is matched filtered to produce an estimate of the channel impulse response. Rather than relying on the size of the physical receive antenna and the corresponding beamwidth to determine the minimum resolvable separation between closely spaced objects, the concept of synthesizing an aperture can be leveraged to yield improved angular resolution. Furthermore, a measurement bandwidth higher than the instantaneous bandwidth of the signal can be synthesized to improve delay resolution.

The premise behind a synthetic aperture channel sounder is that a mechanical positioner moves the receive antenna (also called a probe) to points along a spatial sampling lattice. A conventional heterodyne receiver can be used behind the antenna to detect the signal or a vector network analyzer (VNA). If a VNA is used, then a discrete frequency grid is specified of carrier frequencies. An advantage of the VNA approach is that the channel is illuminated with a uniform power spectral density since each radiated sinusoidal tone is of equal amplitude. With some channel sounding waveform modulations, such as pseudo-random noise sequences, the shape of the signal spectrum allocates more power to some frequencies than others.

In the most general case, the spatial sampling lattice of a synthetic aperture can be arbitrary but in typical cases it is chosen to be planar or cylindrical. At each spatial sample point, the receiver digitizes the antenna output and writes the data to memory. The availability of the digitized receive signal at every spatial sample allows the synthetic aperture to emulate the functionality of an element-level digital beamforming (DBF) array. Fig. 2 depicts the synthetic aperture channel sounder developed by the National Institute of Standards and Technology (NIST) in Boulder, CO. This configuration consists of a WR-28 horn antenna mounted on a precision robotic arm with six degrees of motion.

IV. Conventional Wideband Beamforming

The far-field response in spherical coordinates (θ, ϕ) for a phased array or synthetic aperture of $M \times N$ homogeneous elements located in the xy plane is given by,

$$B(\theta,\phi) = E(\theta,\phi) \sum_{m=0}^{M-1} \sum_{n=0}^{N-1} w_{mn} e^{jk(x_m \sin\theta\cos\phi + y_n \sin\theta\sin\phi)} \tag{1}$$

where $E(\theta,\phi)$ is the array element pattern, the wavenumber $k = 2\pi/\lambda$, λ is the operating wavelength, and w_{mn} is the array element weighting or the measured $S21$ parameter. If the array elements are uniformly spaced on a rectangular grid then the element locations are given by $x_m = md_x$ and $y_n = nd_y$ where d_x and d_y denote the spacing between elements in the x and y directions. This equation can be rewritten as a 2-D spatial Fourier Transform by using the sine space coordinates $u = \sin\theta\cos\phi$ and $v = \sin\theta\sin\phi$,

$$B(u,v) = E(u,v) \sum_{m=0}^{M-1} \sum_{n=0}^{N-1} w_{mn} e^{jk(md_x u + nd_y v)}. \tag{2}$$

The beamforming operation performed in synthetic aperture post-processing forms the coherent sum of all the signals measured across the sampling aperture as described by (1) or (2) to create a directional receive beam in space. This beam may be steered to different directions by applying the appropriate phase shift between successive array elements. To steer the beam in the direction (θ, ϕ) the phase shift applied at the mnth array element is given by

$$\psi_{mn}(\theta,\phi) = \frac{2\pi}{\lambda}(x_m \sin\theta\cos\phi + y_n \sin\theta\sin\phi) \tag{3}$$

where x_m denotes the x-coordinate of the element's location and y_m denotes the y-coordinate.

For wideband applications it is necessary to prevent beam squint by implementing true time-delay beam steering. If the phase shift $\psi_{mn}(\theta_0, \phi_0)$ is computed exactly for an initial frequency ω_0 then at all other frequencies a differential phase shift proportional to the frequency difference is applied. The steering phase versus frequency is then given by

$$\begin{aligned}\psi_{mn}(\omega; \theta_0, \phi_0) &= \psi_{mn}(\omega_0; \theta_0, \phi_0)[1 + (\omega - \omega_0)/\omega_0] \\ &= \psi_{mn}(\omega_0; \theta_0, \phi_0)\omega/\omega_0.\end{aligned} \quad (4)$$

The wideband processing described in Algorithm 1 eliminates beam squint by applying a phase shift proportional to frequency, or equivalently a time delay, at each array element to steer the beam.

True time-delay beam steering refers to the practice of inserting a pure time delay instead of a phase shift behind each array element to steer the beam in wideband arrays. True time-delay beam steering can be implemented on wideband synthetic apertures to avoid beam squint by applying a frequency dependent phase taper to the array output vector as described in (4). After computing the dot product of the beam steering phase taper and the array output vector for every frequency, an Inverse Fourier Transform is computed to yield the beam output power received from the direction (θ_0, ϕ_0) as a function of delay. This beam output is also known as the power delay profile (PDP) for the direction (θ_0, ϕ_0). The process is summarized in Algorithm 1. Note that a frequency invariant beamformer may replace the phase steering vectors $\mathbf{w}(\omega_k; u_0, v_0)$ with optimized weight vectors computed at every frequency for the desired beam-steering direction.

Algorithm 1 PADP and Delay Slice Creation

Input: Array output vector $\mathbf{y}(\omega_k)$ at each frequency ω_k for $k = 0, \ldots, S-1$ and desired beam pointing direction (u_0, v_0)

1: Compute the phase steering vector for each frequency, $\mathbf{w}(\omega_k; u_0, v_0)$.
2: Beamform the array output vector $\mathbf{y}(\omega_k)$ at each frequency by forming the dot product $b(\omega_k; u_0, v_0) = \mathbf{w}(\omega_k; u_0, v_0)^H \mathbf{y}(\omega_k)$
3: Compute the Inverse Fourier Transform (temporal) to obtain the beam output (directional PDP), $x(\tau_k; u_0, v_0) = IFT[b(\omega_k; u_0, v_0)]$
4: To reduce high-frequency, time-domain ripple in wide bandwidth measurements and to increase sampling resolution, compute a window function c_k of length S with low sidelobes, e.g. Hamming window. Then zero-pad the sequence $c_k b(\omega_k; u_0, v_0)$ to L times its original length before computing the IDFT
5: For a fixed delay, $\tau = \tau_0$, $x(\tau_0; u, v)$ is the spatial frequency spectrum of all signal sources impinging on the array (also called a delay slice) and can be used to estimate angles of arrival

Outputs: PDP $x(\tau; u_0, v_0)$ in the fixed direction (u_0, v_0). Delay slice $x(\tau_0; u, v)$ at the fixed delay τ_0.

A. Delay Slices

The wideband true-time-delay algorithm can be leveraged to evaluate delay slices of the four-dimensional channel impulse response by computing directional PDPs at directions (θ_k, ϕ_k) or (u_k, v_k) on a discrete angular grid of $k = 0, \ldots, K-1$ angles that encompass the entire forward hemisphere. If these PDPs are evaluated over all the angles at the fixed delay $\tau = \tau_m$, then $x(\tau_m; u, v)$ is the spatial frequency spectrum of all signal sources impinging on the array and can be used to estimate strong angles of arrival for the delay bin τ_m. The equation for evaluating the Inverse Discrete Fourier Transform of the beam output $b(f_s; u_k, v_k)$ at only the mth delay bin τ_m is

$$x(\tau_m; u_k, v_k) = \frac{1}{S} \sum_{s=0}^{S-1} b(f_s, u_k, v_k) e^{j2\pi ms/S} \quad (5)$$

where S is the total number of frequency samples f_s and $0 \leq m \leq S-1$. Delay slices provide a detailed view of the angular power spectrum created by multipath scattering as a function of time.

V. Spherical Phasefront Wideband Beamforming

Conventional wideband beamforming assumes plane waves with straight-line phasefronts are travelling across the plane of the aperture. In reality however radiated waves propagate radially outward from a signal source as shown in Fig. 3. The spherical curvature of a propagating phasefront is an especially important source of beamforming error for electrically large apertures or at distances close to the aperture. To attain the highest level of prediction accuracy for IRS performance, it is necessary to use spherical beamforming in synthetic aperture post-processing.

In general, the field of a propagating monochromatic plane wave as a function of position $\mathbf{x}$ and time t is given by,

$$U(\mathbf{x}, t) = e^{j2\pi(-\mathbf{v}^T \mathbf{x} + ft)} \quad (6)$$

where $\mathbf{v}$ is the propagation direction (spatial frequency) vector and f is temporal frequency. For a spherical wavefront,

$$U(\mathbf{x}, t) = e^{-j\frac{2\pi}{\lambda} d(\mathbf{x})} e^{j2\pi ft} \quad (7)$$

where $d(\mathbf{x})$ is the distance between the signal source and the receive location $\mathbf{x}$. Spherical beamforming proceeds by using (7) to compute modified steering vectors with phase shifts at each array element that are dependent on the straight-line distance from a signal source to the receive antenna. In this case the beamformed array output becomes,

$$B_{xyz} = \sum_{m=0}^{M-1} \sum_{n=0}^{N-1} w_{mn} e^{jkDmn} \quad (8)$$

where we assume isotropic array elements. D_{mn} represents the straight-line distance from a point signal source with coordinates (s_x, s_y, s_z) to the mnth array element at (x_m, y_n, z),

$$D_{mn} = \sqrt{(s_x - x_m)^2 + (s_y - y_n)^2 + (s_z - z)^2}. \quad (9)$$

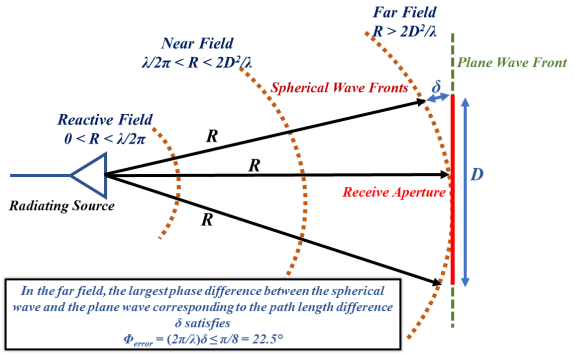

Fig. 3: Spherical wave model.

The planar synthetic aperture is assumed to lie in the xy plane with constant z coordinates. To evaluate (8) over all angles the point source is moved on a circle of constant radius around the receive antenna. Algorithm 2 lists the computational steps for using spherical beamforming to create directional PDPs and delay slices of the channel impulse response.

Algorithm 2 Spherical Phasefront PADP and Delay Slice Creation

Input: Array output vector $\mathbf{y}(\omega_k)$ at each frequency ω_k for $k = 0, \ldots, S-1$ and desired beam pointing direction (Az_0, El_0) corresponding to (u_0, v_0).

1: Starting from an initial range R_0 and proceeding to a final range R_1 in increments of ΔR, compute the Cartesian coordinates (x_k, y_k, z_k) corresponding to the spherical coordinates (R_k, u_0, v_0).

2: Compute the distance from (x_k, y_k, z_k) to each spatial sample in the synthetic aperture.

3: Compute the spherical steering vector, $\mathbf{w}(\omega_k; u_0, v_0, R_k)$, for each frequency. Each component of the spherical steering vector corresponds to the propagation phase e^{jkDmn} where $k = 2\pi/\lambda$. Here (m, n) denotes the indices of each spatial sample in the synthetic aperture and $D_{mn} = \sqrt{(x_k - x_m)^2 + (y_k - y_n)^2 + (z_k - z)^2}$.

4: Stack all the frequency-dependent steering vectors into $\widehat{\mathbf{w}}(\omega; u_0, v_0, R_k)^H$ and all the array output vectors into $\widehat{\mathbf{y}}(\omega)$. Then beamform the wideband array output by forming the dot product $b(u_0, v_0, R_k) = \widehat{\mathbf{w}}(\omega; u_0, v_0, R_k)^H \widehat{\mathbf{y}}(\omega)$

5: Repeat steps 1 through 4 for all angles on a discrete grid at a fixed range R_k to create a delay slice $x(u, v; R_k)$.

VI. Spherical Beamforming Results

This section describes the results of numerical and measured experiments that demonstrate spherical beamforming. In the measurement scenario, two aluminum cylinders with a lateral separation between them were placed on an optical table and measured using a synthetic aperture as shown in Fig. 4. The synthetic aperture consisted of a 35-by-35 planar lattice with 3 mm spacing between sample points. Fig. 5 is a delay slice generated using Algorithm 2 that clearly shows the boresight cylinder. For comparison, Fig. 6 is a simulated delay slice for

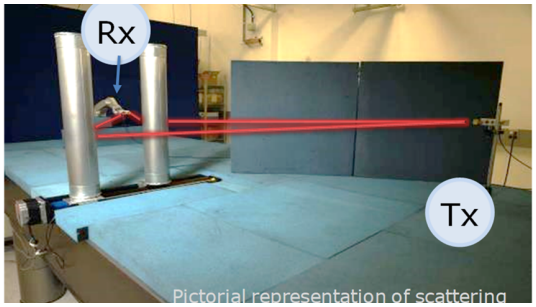

Fig. 4: Scattering experiment using 2 cylinders.

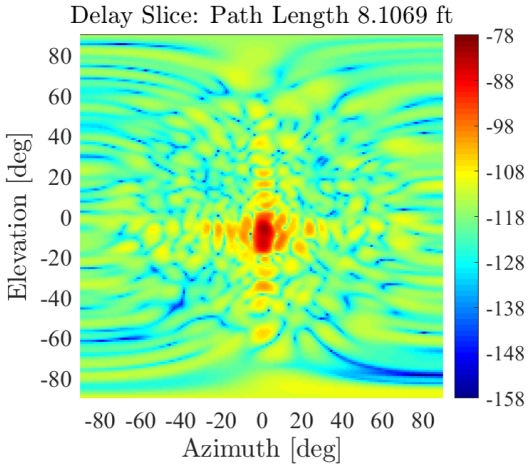

Fig. 5: Wideband delay slice constructed using Algorithm 2.

two cylinders at the same range with different angles of arrival. Fig. 7 is a conventional PDP computed using Algorithm 1 and Fig. 8 is a PDP computed using the spherical beamforming in Algorithm 2. Both PDPs are very similar but differences are visible at early delays corresponding to the near field. Note the nominal far field of the aperture begins at 2.77 m. Algorithm 2 can also be used to compute the scattered field strength for discrete (x, y, z) coordinates in space. Fig. 9 is a top-down view in the X-Z Cartesian plane of the scattered fields in the vicinity of the measured boresight cylinder. Fig. 10 is the corresponding simulation.

VII. Conclusion

Synthetic aperture channel sounders are versatile metrological instruments capable of precisely characterizing millimeter-wave communication channels. This paper describes a novel spherical beamforming approach that leverages synthetic aperture sounding measurements to predict the fields scattered from an IRS placed in a wireless channel to create controlled signal propagation paths.

References

[1] D. Dampahalage, K. B. S. Manosha, N. Rajatheva, and M. Latva-Aho, "Supervised learning based sparse channel estimation for ris aided communications," in *IEEE International Conference on Acoustics, Speech, and Signal Processing (ICASSP)*, May 2022.

[2] S. Idrees, X. Jia, S. Khan, S. Durrani, and X. Zhou, "Deep learning based passive beamforming for irs-assisted monostatic backscatter systems," in *IEEE International Conference on Acoustics, Speech, and Signal Processing (ICASSP)*, May 2022.

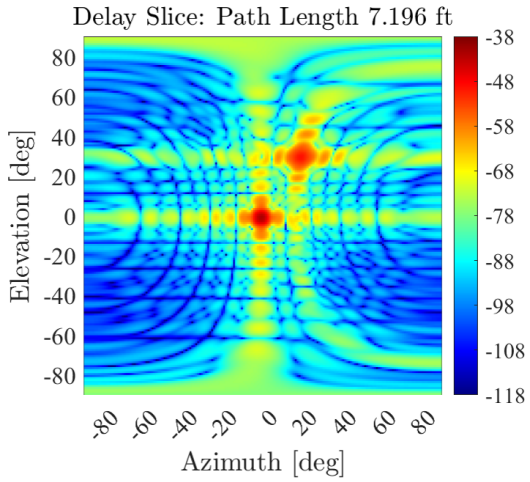

Fig. 6: Simulated delay slice showing 2 cylinders at the same delay.

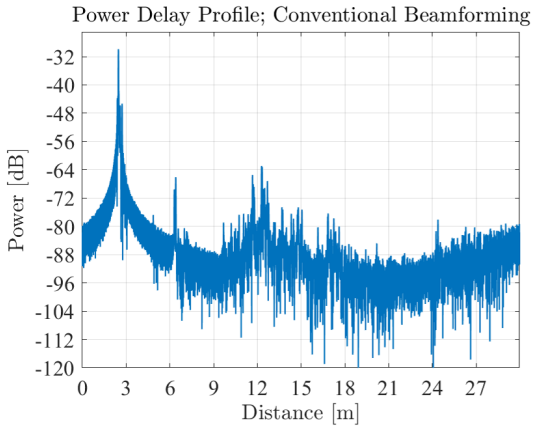

Fig. 7: Conventional wideband PDP in direction of cylinder.

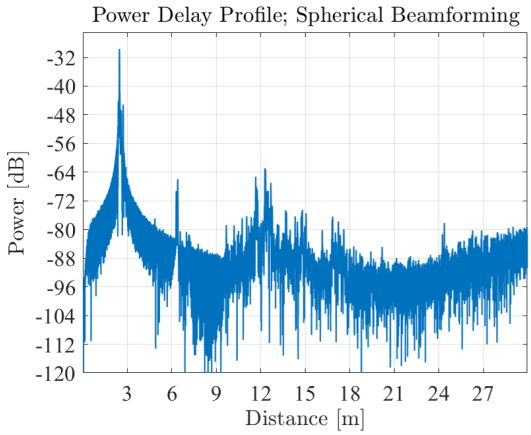

Fig. 8: Spherical PDP in direction of cylinder.

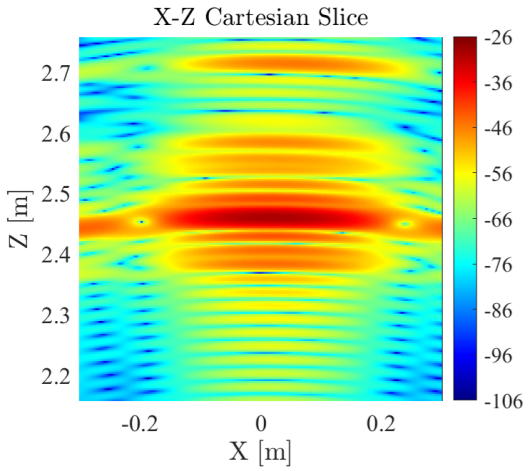

Fig. 9: Measured X-Z Cartesian slice corresponding to top-down view of boresight cylinder; close-up view.

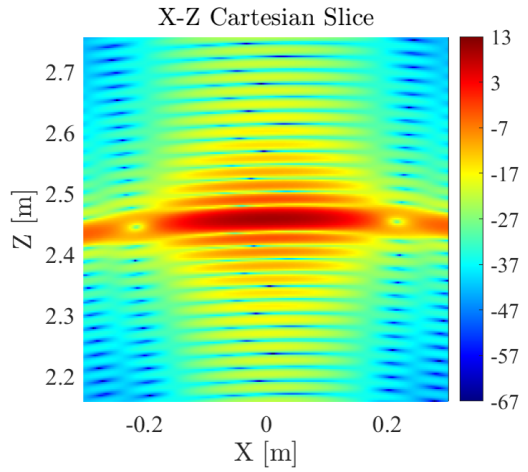

Fig. 10: Simulated X-Z Cartesian slice; close-up view.

[3] K. V. Mishra, A. Chattopadhyay, S. S. Acharjee, and A. P. Petropulu, "Optm3sec: Optimizing multicast irs-aided multiantenna dfrc secrecy channel with multiple eavesdroppers," in *IEEE International Conference on Acoustics, Speech, and Signal Processing (ICASSP)*, May 2022.

[4] F. Karim, B. Hazarika, S. K. Singh, and K. Singh, "A performance analysis for multi-ris-assisted full duplex wireless communication system," in *IEEE International Conference on Acoustics, Speech, and Signal Processing (ICASSP)*, May 2022.

[5] M. Joham, H. Gao, and W. Utschick, "Estimation of channels in systems with intelligent reflecting surfaces," in *IEEE International Conference on Acoustics, Speech, and Signal Processing (ICASSP)*, May 2022.

[6] S. Xu, Y. Du, J. Liu, and J. Li, "Intelligent reflecting surface based backscatter communication for data offloading," *IEEE Trans. Comm.*, April 2022.

[7] L. Xiao, S. Hong, S. Xu, H. Yang, and X. Ji, "Intelligent reflecting surface based backscatter communication for data offloading," *IEEE Trans. Comm.*, April 2022.

[8] J. Ge, Y.-C. Liang, S. Li, and Z. Bai, "Ris-enhanced spectrum sensing: How many reflecting elements are required to achieve a detection probability close to 1," *IEEE Trans. Wireless Comm.*, April 2022.

[9] W. Tan, C. Zhang, J. Peng, L. Dai, S. Fu, and K. Qiu, "Secure transmission via iui engineering for irs-assisted noma systems," *IEEE Wireless Comm. Letters*, April 2022.

[10] J.-B. W. M. Ye, H. Zhang, "Channel estimation for intelligent reflecting surface aided wireless communications using conditional gan," *IEEE Wireless Comm. Letters*, April 2022.